10-1999

An Experimental and Theoretical Study of the Spin–Orbit Interaction for CO+(A 2Π3/2,1/2, v+=0–41) and O+2(X 2Π3/2,1/2g, v+=0–38)

Dmitri G. Fedorov
Iowa State University

M. Evans
Iowa State University

Y. Song
Iowa State University

Mark S. Gordon
Iowa State University, mgordon@iastate.edu

C. Y. Ng
Iowa State University

An Experimental and Theoretical Study of the Spin–Orbit Interaction for CO+(A 2Π3/2,1/2, v+=0–41) and O+2(X 2Π3/2,1/2g, v+=0–38)

Abstract
Accurate spin–orbit splitting constants (Av+) for the vibrational levels v+=0–41 of CO+(A 2Π3/2,1/2) have been determined in a rotationally resolved pulsed field ionization photoelectron study. A change in slope is observed in the v+ dependence for Av+ at v+≈19–20. This observation is attributed to perturbation of the CO+(A 2Π) potential by the CO+(B 2Σ+) state. Theoretical Av+ values for CO+(A 2Π3/2,1/2, v+=0–41) have also been obtained using a newly developed *ab initio* computational routine for spin–orbit coupling calculations. The theoretical Av+ predictions computed using this routine are found to be in agreement with the experimental Av+ values for CO+(A 2Π3/2,1/2, v+=0–41). Similar Av+calculations obtained for O+2(X 2Π3/2,1/2g, v+=0–38) are also in accord with the recent experimental Av+ values reported by Song et al. [J. Chem. Phys. **111**, 1905 (1999)].

Keywords
Ab initio calculations, Field desorption

Disciplines
Chemistry

Comments
The following article appeared in *Journal of Chemical Physics* 111 (1999): 6413, and may be found at doi:10.1063/1.479941.

An experimental and theoretical study of the spin–orbit interaction for CO + (A 2 Π 3/2,1/2 ,v + =0–41) and O 2 + (X 2 Π 3/2,1/2g ,v + =0–38)

D. G. Fedorov, M. Evans, Y. Song, M. S. Gordon, and C. Y. Ng

Citation: The Journal of Chemical Physics **111**, 6413 (1999); doi: 10.1063/1.479941
View online: http://dx.doi.org/10.1063/1.479941
View Table of Contents: http://scitation.aip.org/content/aip/journal/jcp/111/14?ver=pdfcov
Published by the AIP Publishing

An experimental and theoretical study of the spin–orbit interaction for $CO^+(A\,^2\Pi_{3/2,1/2}, v^+=0-41)$ and $O_2^+(X\,^2\Pi_{3/2,1/2g}, v^+=0-38)$

D. G. Fedorov, M. Evans, Y. Song, M. S. Gordon, and C. Y. Ng[a)]
Ames Laboratory, USDOE and Department of Chemistry, Iowa State University, Ames, Iowa 50011

(Received 10 June 1999; accepted 14 July 1999)

Accurate spin–orbit splitting constants (A_{v+}) for the vibrational levels $v^+=0-41$ of $CO^+(A\,^2\Pi_{3/2,1/2})$ have been determined in a rotationally resolved pulsed field ionization photoelectron study. A change in slope is observed in the v^+ dependence for A_{v+} at $v^+ \approx 19-20$. This observation is attributed to perturbation of the $CO^+(A\,^2\Pi)$ potential by the $CO^+(B\,^2\Sigma^+)$ state. Theoretical A_{v+} values for $CO^+(A\,^2\Pi_{3/2,1/2}, v^+=0-41)$ have also been obtained using a newly developed *ab initio* computational routine for spin–orbit coupling calculations. The theoretical A_{v+} predictions computed using this routine are found to be in agreement with the experimental A_{v+} values for $CO^+(A\,^2\Pi_{3/2,1/2}, v^+=0-41)$. Similar A_{v+} calculations obtained for $O_2^+(X\,^2\Pi_{3/2,1/2g}, v^+=0-38)$ are also in accord with the recent experimental A_{v+} values reported by Song *et al.* [J. Chem. Phys. **111**, 1905 (1999)]. © *1999 American Institute of Physics.* [S0021-9606(99)00938-1]

I. INTRODUCTION

The spin–orbit constants (A_{v+}) for the $v^+=0$ and 2 vibrational levels of $CO^+(A\,^2\Pi_{3/2,1/2})$ have been determined to be 122.0 and 121.87 cm^{-1}, respectively,[1,2] which are higher than the value of 117.5 cm^{-1} cited in Huber and Herzberg[3] based on earlier measurements. To our knowledge, the A_{v+} values for the high v^+-levels of $CO^+(A\,^2\Pi_{3/2,1/2}, v^+)$ have not been measured.

The most general experimental method for the determination of A_{v+} values of cations for a wide range of v^+ levels is the photoelectron spectroscopic technique. Due to autoionization mechanisms, photoelectron spectroscopic measurements often allow the observation of highly vibrationally excited states for the cation.[4,5] This is especially the case for threshold photoelectron (TPE) or pulsed field ionization photoelectron (PFI-PE) measurements using a tunable ionization source,[5] where highly vibrational excited ionic states can be observed due to finite couplings to nearby resonance Rydberg states and/or repulsive states. In photoionization studies using a fixed energy light source, such as HeI, highly vibrationally excited ionic states with negligible Franck–Condon factors can also be observed.[4] When the HeI photon energy coincides with the excitation energy of a Rydberg level, the Rydberg level initially formed can decay to a lower vibronic state of the cation, concomitant with the ejection of an energetic electron. This two-step mechanism can thus give rise to a long progression of vibrational bands for the cation, which would not be observed via direct ionization. The HeI spectrum for CO obtained by Wannberg *et al.*[4] indeed reveals high vibrational bands up to $v^+=18$ for $CO^+(A\,^2\Pi)$. However, the two spin–orbit states cannot be resolved in the latter experiment due to the relatively small spin–orbit splitting constant (A_{v+}) for $CO^+(A\,^2\Pi_{3/2,1/2})$. Kong and Hepburn[6] have recently performed a high-resolution vacuum ultraviolet (VUV) laser PFI-PE study of $CO^+(A\,^2\Pi_{3/2,1/2}, v^+=0$ and $1)$. The observed rotationally resolved PFI-PE spectra for these vibrational bands are found to be consistent with $A_{v+}=120\,cm^{-1}$ for $v^+=0$ and 1, which is close to the value of 122 cm^{-1} determined previously.[1,2]

Taking advantage of the high-resolution vacuum ultraviolet (VUV) facility of the chemical dynamics beamline established at the advanced light source (ALS),[7,8] we have recently developed a novel synchrotron based PFI-PE detection scheme,[9,10] achieving PFI-PE resolutions similar to that observed in VUV laser PFI-PE studies.[10–12] The ease of tunability over a wide energy range (6–30 eV) has made this synchrotron based PFI-PE method highly productive, particularly in measuring photoelectron bands of a long vibrational progression. In recent studies, we have reported rotationally resolved PFI-PE bands for long progressions of $O_2^+(X\,^2\Pi_{3/2,1/2g}, v^+=0-38)$,[13] $NO^+(X\,^1\Sigma^+, v^+=0-32)$,[14] and $CO^+(X\,^2\Sigma^+, v^+=0-42)$.[15] Using the same experimental method, we have obtained rotationally resolved PFI-PE spectra for $CO^+(A\,^2\Pi_{3/2,1/2}, v^+=0-41)$. The intensities of PFI-PE bands for higher v^+ (>10) levels of $CO^+(A\,^2\Pi_{3/2,1/2})$ are more than 100 fold lower than those observed for the $v^+=0-2$ bands. Despite the low intensities for the high v^+ bands, we have successfully recorded most of the PFI-PE bands for $CO^+(A\,^2\Pi_{3/2,1/2}, v^+=0-41)$ at the rotationally resolved level with good signal-to-noise ratios. Here, we present accurate A_{v+} values for $CO^+(A\,^2\Pi_{3/2,1/2}, v^+=0-41)$ derived from the analysis of the rotationally resolved PFI-PE spectrum of CO.

In the theoretical front, reliable calculations on spin–orbit interactions have not been readily accessible due to the requirement of accurate electronic and vibrational wave functions. Many theoretical calculations[16–19] have been made

a)Electronic mail: cyng@ameslab.gov

on the potential-energy surfaces of CO^+. The recent multiconfiguration self-consistent field configuration interaction (MCSCF-CI) calculations of Lavendy and Robbe[16] and Okada and Iwata[17] have obtained reliable predictions for the vibrational and rotational constants of $CO^+(A\,^2\Pi_{3/2,1/2})$. However, the A_{v+} value of 92 cm^{-1} for $CO^+(A\,^2\Pi_{3/2,1/2})$ calculated by Lavendy and Robbe[16] is significantly smaller than the experimental measurements[1,2] of 122 cm^{-1}.

In view of the lack of computational routines available for reliable calculations of spin–orbit coupling constants, we have recently developed a new *ab initio* computational code for this purpose. This code, to be included into the production version of the publicly available quantum chemistry package GAMESS,[20] has the capability of performing efficient spin–orbit coupling calculations for arbitrary spin multiplicities with any CI wave function types supported by GAMESS, for both one and two electron spin–orbit coupling operators. As a test of this computational code, we have calculated the A_{v+} values for $CO^+(A\,^2\Pi_{3/2,1/2}, v^+=0-41)$ for comparison with the experimental measurements.

Highly accurate spin–orbit coupling constants for $O_2^+(X\,^2\Pi_{1/2,3/2g}, v^+\leqslant 11)$ have been determined previously[21] in a comprehensive analysis of the $O_2^+(A\,^2\Pi_u) \rightarrow O_2^+(X\,^2\Pi_g)$ emission system. The VUV laser PFI-PE study of Kong and Hepburn has extended the measurement to $O_2^+(X\,^2\Pi_{1/2,3/2g}, v^+=24)$.[22] We note that the A_{v+} values for $O_2^+(X\,^2\Pi_{1/2,3/2g}, v^+=-0-45)$ has also been reported recently in a synchrotron based TPE study.[23] However, the latter A_{v+} values are derived only from vibrationally resolved data. By employing the synchrotron based PFI-PE detection method, Song *et al.* have made a comprehensive spectroscopic study on $O_2^+(X\,^2\Pi_{1/2,3/2g}, v^+=-0-38)$ at the rotational-resolved level,[13] which provides accurate A_{v+} values for these states. Thus, the experimental A_{v+} values for $O_2^+(X\,^2\Pi_{1/2,3/2g})$ can be considered well established. For this reason, we have also obtained theoretical A_{v+} values for this system. The comparison of the theoretical values with experimental A_{v+} data for the $O_2^+(X\,^2\Pi_{1/2,3/2g})$ system serves as a second test case for the new computational code.

II. EXPERIMENTAL AND THEORETICAL METHODS

A. High-resolution PFI-PE measurements

The design and performance of the chemical dynamics beamline at the ALS has been described previously.[7–11] Briefly, the major components for the high-resolution VUV photoionization facility at this beamline include a 10 cm period undulator ($U10$), a gas harmonic filter,[24] a 6.65 m off-plane Eagle mounted monochromator,[8] and a photoelectron–photoion apparatus.[9–11]

In the present experiment, helium was used in the gas harmonic filter, where higher undulator harmonics with photon energies greater than 24.59 eV were suppressed. The fundamental light from the undulator was then directed into the 6.65 m monochromator and dispersed by a 4800 l/mm grating (dispersion=0.32 Å/mm) before entering the experimental apparatus. The ALS storage ring is capable of filling 328 electron buckets in a period of 656 ns. Each electron bucket emits a light pulse of 50 ps with a time separation of 2 ns between successive bunches. In each storage ring period, a dark gap (80 ns) consisting of 40 consecutive unfilled buckets exists for the ejection of cations from the orbit. Thus, the present experiment was performed in the multibunch mode with 288 bunches in the synchrotron orbit, corresponding to a repetition rate of 439 MHz.

The multipurpose photoelectron–photoion apparatus associated with the chemical dynamics beamline was used for the present study.[9–11] A continuous effusive CO beam was produced by a metal orifice (diameter=0.5 mm) at 298 K and a distance of 0.5 cm from the photoionization–photoexcitation (PI/PEX) region. Thus, the rotational temperature of the CO sample is expected to be ≈298 K. We estimate that the CO density at the PI/PEX region is $\approx 10^{-3}$ Torr. The photoionization chamber and photoelectron chamber were evacuated by turbomolecular pumps with pumping speeds of 1200 and 3400 L/s, respectively. The respective pressures maintained in the photoionization chamber and the photoelectron chamber were $\approx 1\times 10^{-5}$ and $\approx 1\times 10^{-7}$ Torr during the experiment.

The PFI-PE detection scheme using the high-resolution monochromatized undulator synchrotron radiation facility at the ALS has been described previously.[9–11] Briefly, a pulsed electric field (height=1.1 V/cm, width=40 ns, delayed by 20 ns with respect to the beginning of the 80 ns synchrotron dark gap) was applied to the repeller at the PI/PEX region. This pulsed electric field was used to field ionize high-n Rydberg species and extract photoelectrons toward the detector and was applied every synchrotron ring period (0.656 μs). An electron spectrometer, which consists of a steradiancy analyzer and a hemispherical energy analyzer arranged in tandem, was used to filter prompt electrons. We have previously shown that PFI-PEs can be detected with little background from prompt electrons after only an 8 ns delay with respect to the beginning of the dark gap.

The achievable PFI-PE resolution depends on the resolution of the excitation VUV light source and the magnitude of the applied pulsed electric field.[10] The PFI-PE spectra for CO presented in this experiment were measured using monochromator slits ranging from 30–200 μm. The PFI-PE resolution achieved was 4–7 cm^{-1} [full width at half maximum (FWHM)]. The photon energy step size and counting time used at each photon energy varied between 0.1–0.3 meV and 3–30 s, respectively.

The PFI-PE spectra for CO were calibrated using the PFI-PE spectra of the $Ar^+(^2P_{3/2})$ and $Ne^+(^2P_{3/2})$ bands obtained at the same experimental conditions. This calibration scheme assumes that the Stark shifts for the IEs of CO and the rare gases are identical. The calibration for the CO PFI-PE spectrum was made before and after the experiment. Our previous experience with energy calibrations of the PFI-PE spectra of other molecular systems indicates that the accuracy of the present energy calibration is within ±0.5 meV.[25] Since the spin–orbit PFI-PE components for individual v^+-levels were recorded in a single scan, the error due to energy calibration does not apply to the uncertainties assigned for the A_{v+} values. Most of the A_{v+} values reported here are based on rotationally resolved data and have uncertainties well within ±2 cm^{-1}.

TABLE I. Parameters[a] for the Morse potential [Eq. (2)] for $CO^+(A\,^2\Pi)$ and $O_2^+(X\,^2\Pi)$ obtained by fitting the *ab initio* potential energies and experimental vibrational energies for $CO^+(A\,^2\Pi_{3/2})$.

Morse potential	R_e (Å)	A (Å^{-1})	D_e (cm^{-1})	ω_e^+ (cm^{-1})	$\omega_e^+\chi_e^+$ (cm^{-1})
Expt $CO^+(A\,^2\Pi_{3/2})$[b]	1.2444	2.3531	45 147	1567.5	13.61
Expt $CO^+(A\,^2\Pi_{1/2})$[b]	1.2444	2.3579	45 006	1568.3	13.66
Expt $CO^+(A\,^2\Pi)$[c]	1.2436	2.345	45 115	1562.1	13.52
Theo $CO(A\,^2\Pi)$[d]	1.2510	2.2585	45 542	1511.1	12.53
Expt $O_2^+(X\,^2\Pi)$[e]	1.1200	2.8343	54 392	1919.1	16.93
Expt $O_2^+(X\,^2\Pi)$[c]	1.1227	2.8008	53 250	1876.4	16.53
Theo $O_2^+(X\,^2\Pi)$[d]	1.1249	2.7915	55 541	1910.0	16.42

[a]R_e is the equilibrium bond distance for $CO^+(A\,^2\Pi,\ v^+=0)$ and D_e=well depth, ω_e^+=vibrational frequency, and $\omega_e^+\chi_e^+$=anharmonicity for the Morse potential.
[b]Morse potential based on experimental vibrational energies for work.
[c]Morse potential based on vibrational constants cited in Ref. 3.
[d]Morse potential based on *ab initio* potential energies calculated in this work.
[e]Morse potential based on experimental vibrational energies of Ref. 13.

B. Spin–orbit coupling calculations

Ab initio spin–orbit coupling calculations have been made possible by generalization of the existing spin–orbit coupling code built into the quantum chemistry package GAMESS.[20] In order to accurately reproduce experimental results, a large basis set (AVTZ, built into MOLPRO)[26–30] and an extensive CI wave function have been used. The orbitals are optimized with complete active space self-consistent field (CASSCF) method, the active space including electrons in 8 orbitals ($2s$ and $2p$ on C and O).[31] Energy values are further refined with single and double excitations from the CASSCF active space into the virtual space using MOLPRO. We have examined the effect of adding single and double excitations from the core $1s$ orbitals into virtual space: The CO^+ results do not include such excitations and the O_2^+ results do. Spin–orbit coupling calculations are performed with the CASSCF wave function and Pauli–Breit Hamiltonian,[32] including rigorous one and two-electron terms and using the modified version of GAMESS soon to be released for distribution. The effect of including neighboring states into spin–orbit coupling diagonalization has been studied. CO^+ calculations include the 6 lowest CI roots and O_2^+ calculations include two roots (i.e., only the $^2\Pi_u$ state).

The potential energy of $CO^+(A\,^2\Pi)$ has been calculated for a series of internuclear C–O distances (R) of interest and a geometry optimization has been performed (at the CASSCF level) to locate the potential minimum. Experimentally, the splitting between the $CO^+(A\,^2\Pi_{3/2})$ and $CO^+(A\,^2\Pi_{1/2})$ spin–orbit states is found as a function of vibrational quantum number up to $v^+=41$. The rotational constants (B_v^+) for $CO^+(A\,^2\Pi_{3/2,1/2},\ v^+=0-41)$ have also been determined. In the first approach, the corresponding average R value $\langle r_{v+}\rangle$ for individual v^+-levels of $CO^+(A\,^2\Pi)$ is estimated using the approximation

$$\langle r_{v+}\rangle=\frac{\hbar}{\sqrt{2\mu B_{v+}}}, \tag{1}$$

where B_v is the rotational constant given by the experiment and μ is the reduced mass of CO^+. At each $\langle r_{v+}\rangle$ value, the spin–orbit coupling constant is computed (the single-point approach). As shown in the discussion below, the A_{v+} constants for $CO^+(^2\Pi_{3/2})$ and $CO^+(^2\Pi_{1/2})$ calculated at these $\langle r_{v+}\rangle$ distances deviate significantly from the experimental values, especially for high v^+ levels.

A more sophisticated approach involves the least-square fit of the calculated *ab initio* potential energies at a series of R values to a Morse potential

$$U(R)=D_e\{1-\exp[-a(R-R_e)]\}^2, \tag{2}$$

where D_e is the well-depth and R_e is the internuclear distance at the potential minimum. The best fitted parameters D_e and a obtained for the Morse potential are listed in Table I. The corresponding vibrational frequency (ω_e) and anharmonicity constant ($\omega_e\chi_e$) for the Morse potential, together with the *ab initio* R_e value for $CO^+(A\,^2\Pi_{3/2,1/2},\ v^+=0)$, are also included in Table I. We note that for a Morse potential only two out of the four parameters (D_e, a, ω_e, $\omega_e\chi_e$) are independent. Since accurate vibrational energies for the $CO^+(A\,^2\Pi_{3/2,1/2},\ v^+=0-41)$ states have also been determined based on the simulation of their PFI-PE bands, we have also constructed a Morse potential to provide the best fit for the experiment vibrational energies of $CO^+(A\,^2\Pi_{3/2,1/2})$. The best fitted parameters for the experimental $CO^+(A\,^2\Pi_{3/2})$ and $CO^+(A\,^2\Pi_{1/2})$ Morse potentials are also given in Table I. We find that these Morse potentials obtained based on the experimental vibrational energies for $CO^+(A\,^2\Pi_{3/2,1/2})$ are in reasonable agreement with the $CO^+(A\,^2\Pi)$ Morse potential based on the *ab initio* calculation. We note that the R_e value and the width of the theoretical $CO^+(A\,^2\Pi)$ Morse potential are greater than the experimental $CO^+(A\,^2\Pi_{3/2,1/2})$ Morse potentials. As a result, the outer turning point of the theoretical Morse potential is greater than that of the experimental Morse potential at the same energy. We also list the Morse potential parameters for $CO^+(A\,^2\Pi)$ constructed based on the vibrational constants cited in Huber and Herzberg.[3] These parameters are in accord with those deduced from the present experiment.

The vibronic wave function used is

$$\Psi^v(r,R)=\Psi_N^v(R)\Psi_e(r,R), \tag{3}$$

where $\Psi_N^v(R)$ is an eigenfunction of the theoretical Morse

potential, $\Psi_e(r,R)$ is the electronic wave function, and r is the electron coordinate. The theoretical A_{v+} value is calculated as,

$$A_{v+} = \int\int \Psi_N^v(R)^+[\Psi_e(r,R)^+ \hat{H}_{PB}\Psi_e(r,R) - \Psi_e'(r,R)^+ \hat{H}_{PB}\Psi_e'(r,R)]\Psi_N^v(R)drdR = \int \Psi_N^v(R)^+ A(R)\Psi_N^v(R)dR, \quad (4)$$

where $\hat{H}_{PB}$ is the Pauli–Breit (PB) Hamiltonian[31] and $\Psi_e(r,R)$ and $\Psi_e'(r,R)$ are the eigenvectors of the H_{PB} matrix in the basis of CASSCF states. The unprimed and primed states correspond to the two levels between which the splitting is calculated (i.e., between $J=\frac{1}{2}$ and $J=\frac{3}{2}$ levels). *Ab initio* splitting constants as a function of R, $A(R)$, are first calculated at discrete R values and then fitted to an appropriate analytical form for the convenience of performing numerical integration. For the $CO^+(A\,^2\Pi_{3/2,1/2})$ system, the $A(R)$ function is found to have the form $A(R)=h(1-\tanh[(R-R_0)s])+A_0$ with the following least-square fit parameters: $h=51.25, A_0=13.5, R_0=2.02, s=3.75$. Here, R and $A(R)$ are in Å and cm^{-1}, respectively.

The average vibrational energies for the $O_2^+(X\,^2\Pi_{3/2,1/2g})$ spin–orbit states have been determined recently in a similar PFI-PE experiment by Song *et al.*[13] The Morse potentials based on fitting to these experimental vibrational energies are given in Table I for comparison with the best fitted *ab initio* Morse potential for $O_2^+(X\,^2\Pi)$. As a reference, we also include in Table I the Morse potential for $O_2^+(X\,^2\Pi)$ based on the vibrational constants cited in Huber and Herzberg.[3] Similar to the observation for the $CO^+(A\,^2\Pi)$ system, the theoretical R_e value is larger than that determined in the experiment. As a result, the other wall of the theoretical Morse potential for $O_2^+(X\,^2\Pi)$ is wider than that for the experimental Morse potential.

The $A(R)$ function associated with Eq. (4) of the $O_2^+(X\,^2\Pi)$ system has the functional form: $A(R)=h\exp[-s(R-R_0)^2]+A_0$. The least-square fit parameters are, $h=138.219, A_0=1.06641, R_0=1.0115$, and $s=58.9876$.

III. RESULTS AND DISCUSSION

A. $CO^+(A\,^2\Pi_{3/2,1/2}, v^+=0-41)$

We have obtained rotationally resolved PFI-PE bands for $CO^+(A\,^2\Pi_{3/2,1/2}, v^+=0-41)$. The bulk of these data and their analysis, including important issues on spectroscopy and photoionization dynamics, will be presented in a future publication.[33] Here, we have selected to show in Figs. 1(a), 1(b), and 2(b) the respective experimental PFI-PE bands (solid circles) for $CO^+(A\,^2\Pi_{3/2,1/2}, v^+=2,15,38)$ to illustrate of the assignment for the spin–orbit components and the typical quality of the simulation. As with the rotational and vibrational constants, the A_{v+} values for $CO^+(A\,^2\Pi_{3/2,1/2}, v^+=0-41)$ are derived from the spectral simulation. The intensities shown for the spectra of Figs. 1(a), 1(b), and 2 reflect the actual relative intensities. As

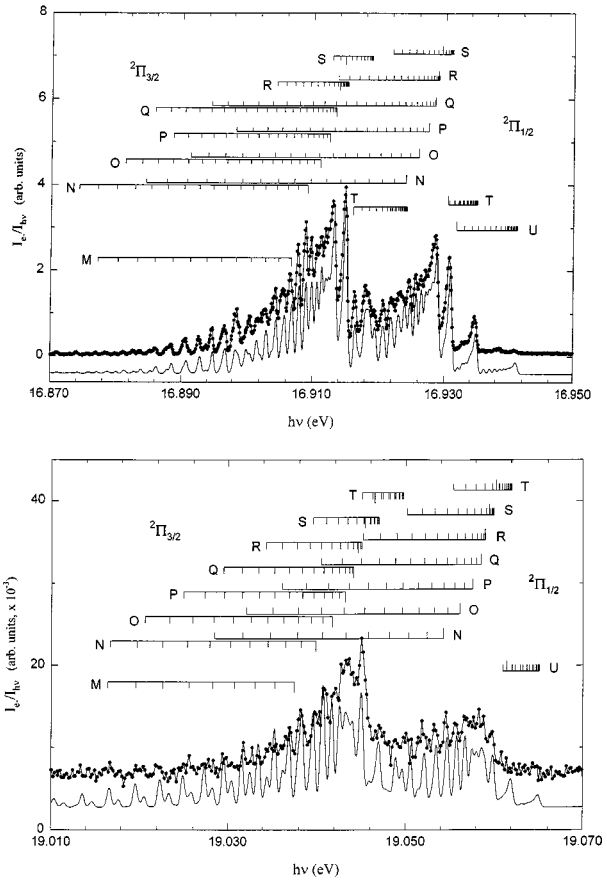

FIG. 1. Comparison of the experimental (solid circles) and BOS simulated (solid line) PFI-PE spectra for (a) $CO^+(A\,^2\Pi_{3/2,1/2}, v^+=2)$ and (b) $CO^+(A\,^2\Pi_{3/2,1/2}, v^+=15)$. Positions for individual rotational are indicated using down pointing and up pointing stick marks for the $^2\Pi_{3/2}$ and $^2\Pi_{1/2}$ components, respectively. The rotational branches are labeled as *M, N, O, P, Q, R, S, T,* and *U* for $\Delta N=-4, -3, -2, -1, 0, 1, 2, 3,$ and 4, respectively. In each ΔN case shown, the position of the first and second transitions are indicated by progressively shorter lines. The PFI-PE resolution achieved $=4\ \mathrm{cm}^{-1}$ (FWHM).

shown in these figures, the intensities for the $CO^+(A\,^2\Pi_{3/2,1/2}, v^+=15 \text{ and } 38)$ bands are more than two orders of magnitude lower that for the $CO^+(A\,^2\Pi_{3/2,1/2}, v^+=2)$ band. We note that the PFI-PE band for $CO^+(A\,^2\Pi_{3/2,1/2}, v^+=38)$ has partial overlap with the $CO^+(X\,^2\Sigma^+, v^+=37)$. Thus, Fig. 2 is a composite figure with panel (a) showing the comparison of the experimental (solid circles) and simulated (solid line) spectra for $CO^+(X\,^2\Sigma^+, v^+=37)$. The analysis and simulation of the PFI-PE bands for $CO^+(X\,^2\Sigma^+, v^+=0-42)$ has been reported previously and thus will not be substantiated here.[13]

The relative intensities for rotational structures resolved in a vibrational band were simulated using the Buckingham–Orr–Sichel (BOS) model,[34] which is described by the formula

$$\sigma(J^+ \leftarrow N'') \propto \Sigma_\lambda Q(\lambda; J^+, N'')C_\lambda. \quad (5)$$

This model was derived to predict rotational line strengths observed in the single-photon ionization of diatomic molecules. Since the BOS model does not take into account channel interactions, which are certain to occur in the

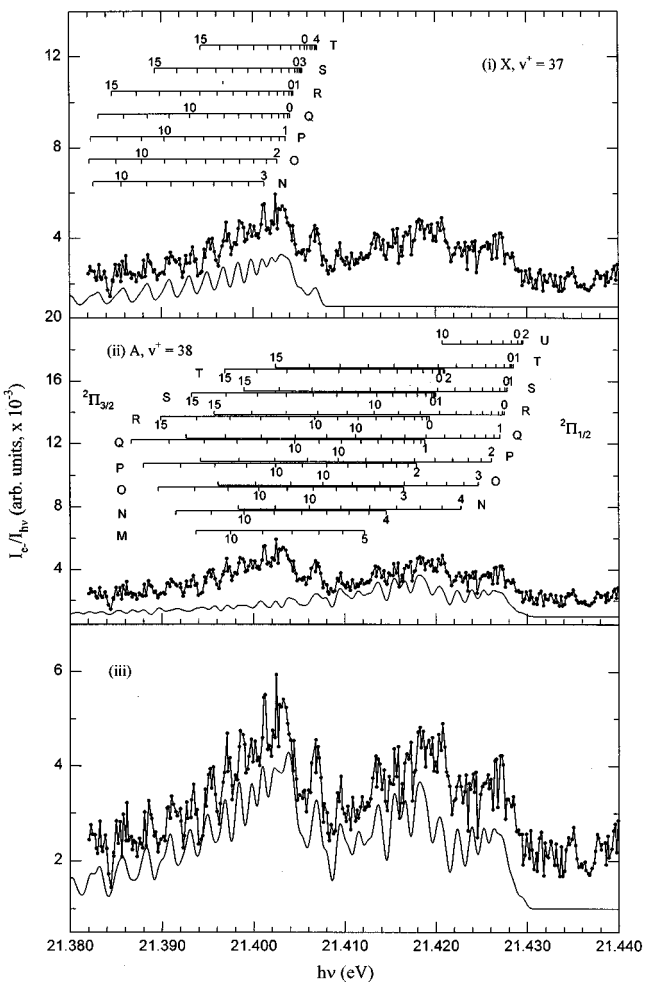

FIG. 2. Composite simulation spectra for $CO^+(X\,^2\Sigma^+,\ v^+=37)$ and $CO^+(A\,^2\Pi,\ v^+=38)$. The figure is divided into three panels. Panel (i) [(ii)] compares the experimental PFI-PE spectrum (solid circles) and the deconvoluted (solid line) PFI-PE spectrum for $CO^+(X\,^2\Sigma^+,\ v^+=37)$ $[CO^+(A\,^2\Pi_{3/2,1/2},\ v^+=38)]$. Panel (iii) compares the experimental (solid circles) PFI-PE spectrum with the sum of the deconvoluted (solid line) spectra for $CO^+(X\,^2\Sigma^+,\ v^+=37)$ and $CO^+(A\,^2\Pi_{3/2,1/2},\ v^+=38)$. In panel (i), positions for individual rotational transitions are indicated by down pointing stick marks. In panel (ii), positions for individual rotational transitions are indicated using down pointing and up pointing stick marks for the $^2\Pi_{3/2}$ and $^2\Pi_{1/2}$ components, respectively. The numbers in panels (i) and (ii) are N'' values. The rotational branches are labeled as *M, N, O, P, Q, R, S, T,* and *U* for $\Delta N=-4,\ -3,\ -2,\ -1,\ 0,\ 1,\ 2,\ 3,$ and 4, respectively. The PFI-PE resolution achieved=4 cm^{-1} (FWHM).

PFI-PE spectra, we may consider the BOS simulation used here as semiempirical in nature. As in previous studies, the BOS simulation is valid in determining spectroscopic constants from the experimental PFI-PE spectra. The factor C_λ is associated with the electronic transition moments, which is the linear combination of electron transition amplitudes for the possible angular momenta l of the ejected electron. The other factor Q is determined by the angular momentum coupling scheme. The parameter λ can be interpreted as the partial wave of the electron in the ground state of the neutral molecule. The more general interpretation of λ is that of the angular momentum transfer in the photoionization process. The angular momentum coupling factor Q for the photoionization of the present CO system can be described by a Hund's case (*b*) to (*a*) transition. The Q factor is thus expressed as

$$Q(\lambda;J^+,N'')=\frac{2J^++1}{2S^++1}\sum_{\chi=|\lambda-1/2|}^{\chi=\lambda+1/2}(2\chi+1)\times\begin{pmatrix}\lambda & S^+ & \chi\\ \Delta\Lambda & \Sigma^+ & \Lambda''-\Omega^+\end{pmatrix}^2\times\begin{pmatrix}J^+ & \chi & N''\\ -\Omega^+ & \Omega^+-\Lambda'' & \Lambda''\end{pmatrix}^2, \tag{6}$$

where $\Delta\Lambda=\Lambda^+-\Lambda''$ and $\Omega^+=|\Lambda^+\pm\Sigma^+|$. Here, Λ^+ and Σ^+ are the projection of the electron orbital angular momentum and electron spin angular momentum on the axis of CO^+, respectively, and Λ'' is the projection of the electron orbital angular momentum on the axis of CO. Given that $\Delta\Lambda=1$ for the transition $CO^+(A\,^2\Pi_\Omega,\ v^+)\leftarrow CO(X\,^1\Sigma^+,\ v''=0)$, the first 3-$j$ symbol of Eq. (6) requires that $\lambda\geqslant 1$. The contribution by each C_λ was determined from the fit to the experimental data. Each spin–orbit state was simulated using a unique set of C_λ's. The rotational structure observed in the experiment was accounted for using the BOS coefficients (C_1, C_2, C_3, and C_4). Thus, the possible angular momentum states for the ejected photoelectron were $l=0$, 1, 2, 3, 4, and 5. The possible change in total angular momentum for a Hund's case (*b*) to (*a*) ionization transition is given by[12]

$$\Delta J=J^+-J''=l+\tfrac{3}{2},l+\tfrac{1}{2},\ldots,-l-\tfrac{3}{2}. \tag{7}$$

Rotational transitions ($\Delta N=N^+-N''$) of -4, -3, -2, -1, 0, 1, 2, 3, and 4 (designated as *M, N, O, P, Q, R, S, T,* and *U* branches, respectively) are clearly observed in the spectra, although transitions up to $\Delta N=\pm 6$ are possible according to Eq. (7).

We assume that the rotational population for CO was characterized by a Boltzmann distribution with a rotational temperature of 298 K. The simulation uses known spectroscopic constants for the molecular ground-state $CO(X\,^1\Sigma^+,v^+)$: $\omega_e''=2169.813\,58$ cm^{-1}, $\omega_e\chi_e''=13.288\,31\,cm^{-1}$, $B_e''=1.931\,28\,cm^{-1}$, and $\alpha_e''=0.0175\,04\,cm^{-1}$.[3] The spin-rotational splitting present in the ionic state has been ignored since it is much smaller than the experimental PFI-PE resolution.

In addition to the BOS C_λ coefficients, the rotational constant B_v^+ and the spin–orbit coupling constant A_{v+} were varied during the simulation of each vibration level. The simulated spectra (solid line, lower spectra) shown in Figs. 1(a), 1(b), and 2(b) were obtained using a Gaussian profile with a linewidth of 4, 4, and 7 cm^{-1} (FWHM), respectively. The positions of the rotational transitions $CO^+(A\,^2\Pi_{3/2},\ v^+,N^+)\leftarrow CO(X\,^1\Sigma^+,\ v''=0,N'')$ and $CO^+(A\,^2\Pi_{1/2},\ v^+,N^+)\leftarrow CO(X\,^1\Sigma^+,\ v''=0,N'')$ are shown by, respectively, downward pointing and upward pointing stick marks in Figs. 1(a), 1(b), and 2(b). As shown in Figs. 1(a) and 1(b), the agreement between the BOS simulated spectra and the experiment PFI-PE spectra are excellent, yielding values of $120.2\pm 2.0\,cm^{-1}$ for $A_{v+}(v^+=2)$, and $117.0\pm 2.0\,cm^{-1}$ for $A_{v+}(v^+=15)$. The $A_{v+}(v^+=2)$ value is in excellent accord

TABLE II. Comparison of the experimental and theoretical spin–orbit constants [A_{v+} (cm^{-1})] for $CO^+(A\,^2\Pi_{3/2,1/2}, v^+=0-41)$ and $O_2^+(X\,^2\Pi_{3/2,1/2g}, v^+=0-38)$.

	A_{v+} (cm^{-1})			
v^+	Expt[$CO^+(A\,^2\Pi)$][a]	Theo[$CO^+(A\,^2\Pi)$][b]	Expt[$O_2^+(X\,^2\Pi)$][c]	Theo[$O_2^+(X\,^2\Pi)$][b]
0	120.2	115.7(116.0)	200.2	195.0(195.1)
1	121.0	115.6(116.0)	199.5	194.4(194.8)
2	120.2	115.5(116.0)	199.0	193.7(194.5)
3	120.2	115.4(115.9)	198.5	193.0(194.2)
4	121.0	115.3(115.8)	197.6	192.2(193.9)
5	122.6	115.2(115.8)	198.0	191.4(193.7)
6	120.2	115.1(115.8)	196.6	190.6(193.2)
7	120.2	114.9(115.7)	195.0	189.7(192.8)
8	120.2	114.7(115.7)	193.1	188.8(192.4)
9	119.4	114.5(115.6)	192.5	187.8(192.0)
10	116.1	114.2(115.6)	192.2	186.8(191.6)
11	120.2	113.9(115.5)	191.0	185.8(191.4)
12	119.4	113.5(115.5)	190.0	184.7(190.7)
13	117.0	113.1(115.4)	189.4	183.5(190.3)
14	119.4	112.6(115.4)	188.0	182.3(189.8)
15	117.0	112.0(115.3)	187.0	181.0(189.3)
16	117.0	111.3(115.3)	185.0	179.8(188.7)
17	117.0	110.5(115.2)	183.5	178.4(188.2)
18	117.0	109.6(115.2)	183.0	177.0(187.6)
19	119.4	108.5(115.2)	179.3	175.5(187.0)
20	⋯	107.3	182.0	173.9(186.3)
21	⋯	105.8	177.0	172.3(185.3)
22	109.7	104.2(116.5)	174.0	170.6(185.3)
23	⋯	102.3	173.0	168.9(184.2)
24	103.2	100.3(130.4)	169.0	167.0(183.1)
25	101.6	98.0(111.0)	168.0	165.1(182.2)
26	99.2	95.5(111.4)	165.0	163.1(182.2)
27	96.0	92.8(111.4)	163.0	161.1(181.4)
28	94.4	90.0(111.2)	161.0	159.0(180.4)
29	91.1	86.9(110.9)	159.0	156.7(179.5)
30	88.7	83.8(110.6)	155.0	154.4(179.0)
31	85.5	80.6(108.9)	155.0	152.0(177.4)
32	83.1	77.4(108.7)	150.0	149.5(175.6)
33	81.5	74.2(107.6)	147.0	147.0(174.4)
34	77.4	71.0(106.7)	146.0	144.3(173.0)
35	74.2	67.9(105.9)	144.0	141.5(173.7)
36	70.2	64.9(105.0)	141.0	138.6(171.6)
37	67.8	61.9(103.7)	142.0	135.7(173.0)
38	66.1	59.1(102.2)	141.0	132.6(169.3)
39	⋯	56.4	⋯	⋯
40	59	53.7(96.0)	⋯	⋯
41	57	51.2(92.8)	⋯	⋯

[a]This work. Experimental A_{v+} values for $CO^+(A\,^2\Pi_{3/2,1/2}, v^+=0-41)$.
[b]This work. Theoretical A_{v+} values for $CO^+(A\,^2\Pi_{3/2,1/2}, v^+=0-41)$ or $O_2^+(X\,^2\Pi_{3/2,1/2g}, v^+=0-38)$ calculated using the *ab initio* Morse potential. Values in parentheses are obtained by the single-point approach based on the $\langle r_e \rangle$ value calculated using Eq. (1).
[c]Reference 13. Experimental A_{v+} values for $O_2^+(X\,^2\Pi_{3/2,1/2})$.

with the literature value of 121.87 cm^{-1}.[2] The comparison of the BOS simulated (solid line) and experimental (solid circles) PFI-PE band for $CO^+(A\,^2\Pi_{1/2}, v^+=38)$ is shown in Fig. 2(b). The sum of the simulated spectra for $CO^+(X\,^2\Sigma^+, v^+=37)$ shown in Fig. 2(a) and $CO^+(A\,^2\Pi_{1/2}, v^+=38)$ gives the overall simulated spectrum (solid line) in Fig. 2(c), which is again in excellent accord with the experimental PFI-PE spectrum (solid circles). The A_{v+} value for $CO^+(A\,^2\Pi_{3/2,1/2}, v^+=38)$ is determined to be $66.1\pm3.0\,cm^{-1}$.

The A_{v+} values for $CO^+(A\,^2\Pi_{1/2}, v^+=0-41)$ obtained in the BOS simulation are listed in Table II. The plot of the experimental A_{v+} value versus v^+ is shown in Fig. 3. It is interesting to note that the A_{v+} value seems to remain nearly constant until $v^+\approx19$, which has an IE value of 19.6 eV. Then it decreases nearly linearly toward higher v^+. Although the A_{v+} values for $CO^+(A\,^2\Pi_{3/2,1/2}, v^+=20, 21,$ and 23) were not determined in the present experiment due to serious overlap with the $CO^+(B\,^2\Sigma^+, v^+=0-2)$ bands, the plot of Fig. 3 seems to reveal a break or a change in slope at $v^+\approx19$ to 20. This may be indicative of perturbation by other states.

Figure 4 depicts the PFI-PE spectrum for CO in the region of 18.5–20.7 eV. The positions of v^+ levels for

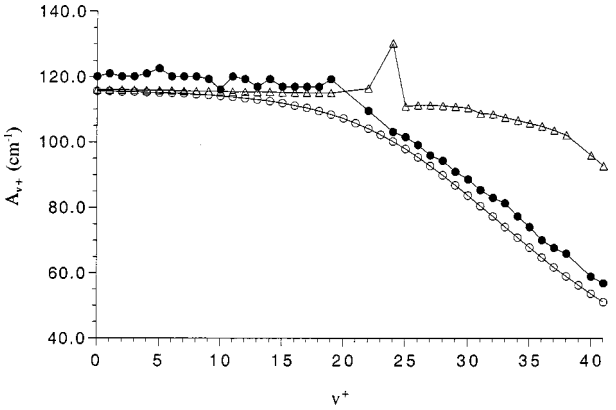

FIG. 3. Plot of the experimental and theoretical spin–orbit splitting constants (A_{v+}) for $CO^+(A\,^2\Pi_{3/2,1/2})$ versus v^+ in the range of $v^+=0-41$. Experimental values are in solid circles. The theoretical values obtained using the *ab initio* Morse potential and by the single-point approach are shown as open circles and triangles, respectively.

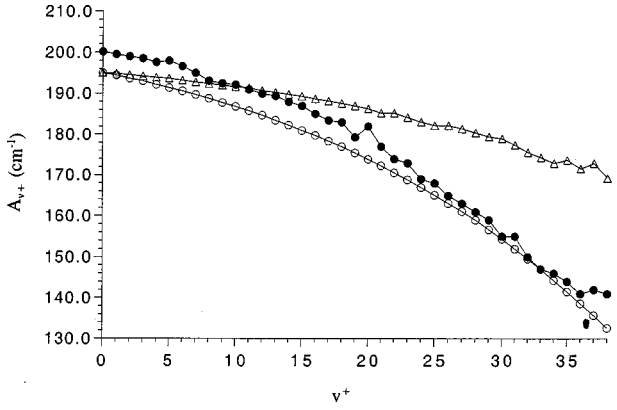

FIG. 5. Plot of the experimental and theoretical spin–orbit splitting constants (A_{v+}) for $O_2^+(A\,^2\Pi_{3/2,1/2})$ versus v^+ in the range of $v^+=0-38$. Experimental values are in solid circles. The theoretical values obtained using the *ab initio* Morse potential and by the single-point approach are shown as open circles and triangles, respectively.

$CO^+(X\,^2\Sigma^+, A\,^2\Pi_{3/2,1/2}, B\,^2\Sigma^+)$ are marked in the figure. We note the overlap of the weak $CO^+(A\,^2\Pi_{3/2,1/2}, v^+=19$ and $20)$ PFI-PE bands with the overwhelmingly strong vibrational band for $CO^+(B\,^2\Sigma^+, v^+=0)$ at 19.80 eV. This observation suggests that the break observed for the v^+ dependence of A_{v+} may arise from high-order interactions between the $CO^+(A\,^2\Pi, v^+=19$ and $20)$ and $CO^+(B\,^2\Sigma^+, v^+=0)$ states. By symmetry, the $CO^+(A\,^2\Pi)$ and $CO^+(B\,^2\Sigma^+)$ can mix by spin–orbit interaction.

Included in Table II are the theoretical A_{v+} values obtained based on the theoretical Morse potential and the single-point approach. We have also plotted in Fig. 3 these theoretical A_{v+} values. As shown in Fig. 3, for $v^+\leqslant 19$ the single-point theoretical predictions and the experimental results are in slightly better accord than those obtained based on the theoretical Morse potential. However, the predictions for $v^+>19$ obtained by the single-point approach deviate significantly lower from the experimental values. This discrepancy observed at high v^+ is expected and can be attributed to the increasing anharmonicity of the $CO^+(A\,^2\Pi)$ potential at high v^+. That is, the $\langle r_e\rangle$ values calculated using the approximation of Eq. (1) are not valid at high v^+ levels, yielding significantly smaller values than the actual equilibrium bond distances for high v^+ levels. The theoretical predictions obtained using the theoretical Morse potential show the correct overall v^+ dependence for A_{v+}. The theoretical A_{v+} value varies smoothly over the whole v^+ range. Contrary to the experimental observation, the v^+ dependence for the theoretical A_{v+} values shows no break at $v^+\approx 19$ to 20.

We find that all theoretical A_{v+} values obtained based on the theoretical Morse potential are slightly lower than the corresponding experimental values. Upon comparing the theoretical and experimental Morse potentials, we find that the *ab initio* R_e value is larger than the experiment R_e value. Furthermore, the outer wall of the *ab initio* Morse potential is softer than that of the experimental Morse potential. That is, at the same energy, the outer turning point for the *ab initio* Morse potential lies at a larger R than that for the experimental Morse potential. As a result, the theoretical Morse potential predicts a larger value for the average equilibrium distance for a given v^+ than that of the experimental Morse potential. This analysis indicates that the lower theoretical predictions compared to the experimental results can be partly ascribed to finite inaccuracy of the *ab initio* Morse potential.

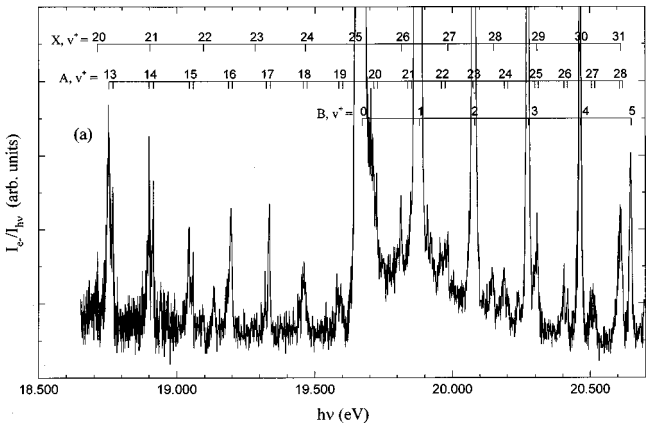

FIG. 4. PFI-PE spectrum for CO in the energy region of 18.5–20.7 eV. The positions of v^+ levels for $CO^+(X\,^2\Sigma^+, A\,^2\Pi_{3/2,1/2}, B\,^2\Sigma^+)$ are marked in the figure. Note that the overlap of the weak $CO^+(A\,^2\Pi_{3/2,1/2}, v^+=19$ and $20)$ PFI-PE bands with the overwhelmingly strong vibrational band for the $CO^+(B\,^2\Sigma^+)$ at 19.80 eV.

B. $O_2^+(X\,^2\Pi_{3/2,1/2g}, v^+=0-38)$

The theoretical A_{v+} predictions obtained here based on the single-point approach and the *ab initio* Morse potential are listed in Table I and plotted in Fig. 5 for comparison with the experimental A_{v+} values for $O_2^+(X\,^2\Pi_{3/2,1/2g}, v^+=0-38)$. The latter values have been reported recently by Song *et al.*[13] Similar to the comparison of the $CO^+(A\,^2\Pi)$ system, the single-point predictions are slightly closer to the experimental results at low $v^+(<19)$. However, contrary to the experimental observation, the slope for the single-point A_{v+} prediction versus $v+$ plot remains nearly constant over the entire range of $v^+=0-38$. That is, the single-point predictions are significantly higher than the corresponding ex-

perimental values at higher $v^+(>21)$ levels. This observation can also be attributed to the inaccuracy of using Eq. (1) for the prediction of $\langle r_e \rangle$ values at high v^+-levels.

The trend of the v^+ dependence for the theoretical A_{v+} value obtained using the *ab initio* Morse potential is consistent with the experimental data. Although the theoretical predictions based on the *ab initio* Morse potential and experimental A_{v+} values are in general agreement, all theoretical predictions are slightly lower than the corresponding experimental results. The comparison of the *ab initio* and experimental Morse potentials are similar to the situation of the $CO^+(A\,^2\Pi)$ system. That is, the outer wall of the theoretical Morse potential is shifted to the longer range compared to that of the experimental Morse potential. Thus, this partly contributes to the lower calculated A_{v+} values.

The A_{v+} values for $O_2^+(X\,^2\Pi_{3/2,1/2g}, v^+=20)$ determined in both the synchrotron based PFI-PE[13] and VUV laser[22] PFI-PE studies are higher than the A_{v+} values for the adjacent $v^+=19$ and 20 states. Thus, the variation of A_{v+} versus v^+ is most likely not a smooth function (see Fig. 5). We note that this kink observed at $O_2^+(X\,^2\Pi_{3/2,1/2g}, v^+=20)$ with an IE$\approx$15.96 eV is also close to the beginning of the vibrational progression of the $O_2^+(a\,^4\Pi_u)$ state beginning at $\approx$16.10 eV. The latter PFI-PE band is nearly in total overlap with the $O_2^+(X\,^2\Pi_{3/2,1/2g}, v^+=21)$ state. The A_{v+} values for $O_2^+(X\,^2\Pi_{3/2,1/2g}, v^+=37$ and $38)$, which have the IEs $\approx$17.9–18.0 eV, also seem to deviation from the general trend of the A_{v+} versus v^+ curve. This observation may be correlated to the appearance of the vibrational progression for the $O_2^+(b\,^4\Sigma_g^-)$ state at 18.1 eV. On the basis of this observation, we tentatively attribute this kink at $O_2^+(X\,^2\Pi_{3/2,1/2g}, v^+=20)$ and $O_2^+(X\,^2\Pi_{3/2,1/2g}, v^+=37$ to 38) as due to perturbation by the $O_2^+(a\,^4\Pi_u)$ and $O_2^+(b\,^4\Sigma_g^-)$ states, respectively. This speculation requires theoretical confirmations in the future.

The effect of core excitations is noticeable mostly at large distances near the dissociation limit where the core excitation become essential to obtain a good energy curve. The Morse potential parameters are noticeably better for O_2^+ where the excitations have been included. The inclusion of other low lying states of CO^+, most noticeably, $X\,^2\Sigma^+$, gives an opportunity to theoretically verify the experimentally seen features in spin–orbit splitting. Since the Morse potential approach is based upon the single state results it displays a smooth dependence without any jumps. The single point approach, on the other hand, allows to study the effect of other states. The calculated jump in spin–orbit splitting at $v^+=24$ is due to interaction with the $X\,^2\Sigma^+$ state. However here the *ab initio* method experiences difficulties associated with having to obtain accurate wave function for both $X\,^2\Sigma^+$ and $A\,^2\Pi$ states. Two possible solutions exist: State-averaging between the two states of interest or using a feature of our code to do spin–orbit coupling with nonorthogonal separate sets of orbitals. To be consistent with the rest of calculations we choose to optimize orbitals only for the $A\,^2\Pi$ state and use these orbitals to obtain the wave function for the other state. This causes a somewhat overestimated jump in the splitting.

IV. CONCLUSIONS

We have obtained accurate A_{v+} constants for $CO^+(A\,^2\Pi_{3/2,1/2}, v^+=0-41)$ in a rotationally resolved PFI-PE experiment. A break at $CO^+(A\,^2\Pi_{3/2,1/2}, v^+\approx 19$ to 20) was observed in the plot of A_{V+} versus v^+. Such a feature is tentatively interpreted as due to perturbation of the $CO^+(B\,^2\Sigma^+)$ state. We have also identified similar features in the v^+ dependence of A_{v+} values for $O_2^+(X\,^2\Pi_{3/2,1/2g}, v^+=0-38)$, suggesting perturbation from the $O_2^+(A\,^2\Pi_u)$ and $O_2^+(b\,^4\Sigma_g^-)$ states.

We have also developed a new *ab initio* computational code for reliable spin–orbit coupling calculations. The A_{v+} predictions for $CO^+(A\,^2\Pi_{3/2,1/2}, v^+=0-41)$ and $O_2^+(X\,^2\Pi_{3/2,1/2g}, v^+=0-38)$ obtained using this computation routine are found to be in agreement with experimental measurements.[13]

The systematic underestimation of the theoretical values for the splitting relative to the experimental values is attributed to two factors of the same order of importance: The first-order perturbative treatment of spin–orbit coupling and the complete omission of the spin–spin coupling. To assert the effect of a larger CI expansion upon the spin–orbit coupling we have performed spin–orbit coupling calculations with single excitations from the CAS into the virtual space at equilibrium, near the dissociation limit and at a middle point. The splitting decreased by about 4 cm^{-1} except for the dissociation limit where the change was 8 cm^{-1}. Thus, the agreement with experiment is found to be worse with the inclusion of the single excitations. Single and double excitations are several million in number and are not possible computationally unless some kind of contraction scheme is employed.

ACKNOWLEDGMENTS

This work was supported by the Director, Office of Energy Research, Office of Basic Energy Sciences, Chemical Science Division of the U.S. Department of Energy under Contract No. W-7405-Eng-82 for the Ames Laboratory, and Contract No. DE-AC03-76SF00098 for the Lawrence Berkeley National Laboratory. Y.S. is the recipient of the 1999 Wall Fellowship at Iowa State University.

[1] D. H. Katayama and J. A. Walsh, J. Chem. Phys. **75**, 4224 (1981).
[2] H. Gagmaire and J. P. Goure, Can. J. Chem. **54**, 2111 (1976).
[3] K. P. Huber and G. Herzberg, *Molecular Spectra and Molecular Structure, Vol. IV, Constants of Diatomic Molecules* (Van Nostrand, New York, 1979).
[4] B. Wannberg, D. Nordfors, K. L. Tan, L. Karlsson, and L. Mattsson, J. Electron. Spectros. Relat. Phenom. **47**, 147 (1988).
[5] P.-M. Guyon and T. Baer, in *High Resolution Laser Photoionization and Photoelectron Studies*, edited by I. Powis, T. Baer, and C. Y. Ng, Wiley Series in Ion Chemistry and Physics (Wiley, Chichester, 1995), Chap. 1.
[6] W. Kong and J. W. Hepburn, J. Phys. Chem. **99**, 1637 (1995).
[7] C.-W. Hsu, M. Evans, P. Heimann, K. T. Lu, and C. Y. Ng, J. Chem. Phys. **105**, 3950 (1996).
[8] P. Heimann, M. Koike, C.-W. Hsu, M. Evans, K. T. Lu, C. Y. Ng, A. Suits, and Y. T. Lee, Rev. Sci. Instrum. **68**, 1945 (1997).
[9] C.-W. Hsu, M. Evans, P. A. Heimann, and C. Y. Ng, Rev. Sci. Instrum. **68**, 1694 (1997).
[10] C.-W. Hsu, M. Evans, S. Stimson, C. Y. Ng, and P. Heimann, Chem. Phys. **231**, 121 (1998).

[11] C. Y. Ng, in *Photoionization and Photodetachment*, edited by C. Y. Ng, Adv. Ser. Phys. Chem. (World Scientific, Singapore, 1999), Vol. 10A (in press).
[12] ''High Resolution Laser Photoionization and Photoelectron Studies,'' *Wiley Series in Ion Chem. and Phys.* edited by I. Powis, T. Baer, and C. Y. Ng (Wiley, Chichester, 1995).
[13] Y. Song, M. Evans, C. Y. Ng, C.-W. Hsu, and G. K. Jarvis, J. Chem. Phys. **111**, 1905 (1999).
[14] G. K. Jarvis, M. Evans, C. Y. Ng, and K. Mitsuke, J. Chem. Phys. **111**, 3058 (1999).
[15] M. Evans and C. Y. Ng, J. Chem. Phys. (accepted).
[16] H. Lavendy and J. M. Robbe, Chem. Phys. Lett. **205**, 456 (1993).
[17] K. Okada and S. Iwata, J. Chem. Phys. (submitted).
[18] N. Honjou and Sasaki, Mol. Phys. **37**, 1593 (1978).
[19] M. E. Wacks, J. Chem. Phys. **41**, 930 (1964).
[20] M. W. Schmidt, K. K. Baldridge, J. A. Boatz, S. T. Elbert, M. S. Gordon, J. H. Jensen, S. Koseki, N. Matsunaga, K. A. Nguyen, S. J. Su, T. L. Windus, M. Dupuis, and J. A. Montgomery, J. Comput. Phys. **14**, 1347 (1993).
[21] J. A. Coxon and M. P. Haley, J. Mol. Spectrosc. **108**, 119 (1984).
[22] W. Kong and J. W. Hepburn, Can. J. Chem. **72**, 1284 (1994).
[23] T. Akahori, Y. Morioka, T. Tanaka, H. Yoshii, T. Hayaishi, and K. Ito, J. Chem. Phys. **107**, 4875 (1997).
[24] A. G. Suits, P. Heimann, X. Yang, M. Evans, C.-W. Hsu, D. A. Blank, K.-T. Lu, A. Kung, and Y. T. Lee, Rev. Sci. Instrum. **66**, 4841 (1995).
[25] S. Stimson, Y.-J. Chen, M. Evans, C.-L. Liao, C. Y. Ng, C.-W. Hsu, and P. Heimann, Chem. Phys. Lett. **289**, 507 (1998).
[26] MOLPRO is a package of *ab initio* programs written by H.-J. Werner and P. J. Knowles, with contributions from J. Almlöf, R. D. Amos, M. J. O. Deegan, S. T. Elbert, C. Hampel, W. Meyer, K. Meyer, K. Peterson, R. Pitzer, A. J. Stone, P. R. Taylor, and R. Lindh.
[27] H.-J. Werner and P. J. Knowles, J. Chem. Phys. **82**, 5053 (1985).
[28] P. J. Knowles and H.-J. Werner, Chem. Phys. Lett. **115**, 259 (1985).
[29] H.-J. Werner and P. J. Knowles, J. Chem. Phys. **89**, 5803 (1988).
[30] P. J. Knowles and H.-J. Werner, Chem. Phys. Lett. **145**, 514 (1988).
[31] M. W. Schmidt and M. S. Gordon, Annu. Rev. Phys. Chem. **49**, 233 (1998).
[32] H. A. Bethe and E. E. Salpeter, *Quantum Mechanics of the One and Two Electron Atoms* (Plenum, New York, 1977).
[33] M. Evans and C. Y. Ng, J. Chem. Phys. (in preparation).
[34] A. D. Buckingham, B. J. Orr, and J. M. Sichel, Philos. Trans. R. Soc. London, Ser. A **268**, 147 (1970).